FROM PRIMAL SKETCHES TO THE RECOVERY OF INTENSITY AND REFLECTANCE REPRESENTATIONS

Rachel Alter-Gartenberg*
Old Dominion University, Norfolk, Virginia

Ramkumar Narayanswamy
Science and Technology Corporation, Hampton, Virginia

and

Karen S. Nolker
Computer Sciences Corporation, Hampton, Virginia

ABSTRACT

A local change in intensity (edge) is a characteristic that is preserved when an image is filtered through a bandpass filter. Primal sketch representations of images, using the bandpass-filtered data, have become a common process since Marr proposed his model for early human vision. In this paper, we move beyond the primal sketch extraction to the recovery of intensity and reflectance representations using only the bandpass-filtered data.

Assessing the response of an ideal step edge to the Laplacian of Gaussian ($\nabla^2 G$) filter, we have found that the resulting filtered data preserves the original change of intensity that created the edge in addition to the edge location. Using the filtered data, we can construct the primal sketches and recover the original (relative) intensity levels between the boundaries. Similarly, we found that the result of filtering an ideal step edge with the Intensity-Dependent Spatial Summation (IDS) filter preserves the actual intensity on both sides of the edge, in addition to the edge location. The IDS filter also preserves the reflectance ratio at the edge location. Therefore, we can recover the intensity levels between the edge boundaries as well as the (relative) reflectance representation. The recovery of the reflectance representation is of special interest as it erases shadowing degradations and other dependencies on temporal illumination.

This method offers a new approach to low-level vision processing as well as to high data-compression coding. High compression can be gained by transmitting only the information associated with the edge location (edge primitives) that is necessary for the recovery process.

1. INTRODUCTION

Primal sketches have become an important method of image description for low-level vision. One approach commonly used to produce these sketches is to bandpass filter the image data and then use the antisymmetrical signals created around intensity transitions (edges) to find their boundary location. We call the antisymmetrical signal a Mach-band pattern because it resembles the visual perception of an edge known as Mach-bands.[1] In this paper, we show that the Mach-band patterns contain more information about the original target than just the edge location. This additional information allows us to move beyond

* Mailing address: NASA Langley Research Center, MS 473, Hampton, VA

the extraction of primal sketches to the recovery of intensity and reflectance representations. Figure 1 demonstrates the recovery process of the intensity representation from the bandpass-filtered data for both a computer-generated target and a sampled image (e.g., image that is degraded by aliasing, blurring, and noise). The bandpassed images (b) of the targets (a) exhibit the familiar Mach-band patterns around the intensity transitions. Using the information contained in the Mach-band patterns we can recover the locations of the intensity transitions and extract the primal sketches (c) together with the actual change of intensity there. The recovery process uses this additional information to recover the original target (a), using only the bandpassed data (b) as is illustrated in (d).

The conditions that allow us to recover a signal from partial information and specifically, the relationship between signals and their zero crossings, have been of considerable interest in the past. Logan[2] has set the conditions under which one-dimensional bandpass signals are uniquely specified by their zero crossings. Curtis et al.[3] set the conditions under which real, continuous, periodic, band-limited two-dimensional signals are specified from the zero-crossing locations of the real part of their Fourier transform. They applied their results to recover simple images from their threshold crossings. Independently, Yuille and Poggio,[4] and Hummel[5] showed that in the absence of image-gathering degradations, a target could be uniquely recovered from the information contained in its second derivative.

In this paper we assess the response of an ideal step edge to two models for retinal processing in human vision. We have found that the Mach-band pattern that results from filtering an ideal step edge with the $\nabla^2 G$ filter[6] preserves the original change of intensity that created the edge, in addition to the edge location (the zero-crossing location). Therefore, we can construct the primal sketches and recover the (relative) intensity levels between the boundaries. Similarly, we have found that the Mach-band pattern that results from filtering an ideal step edge with the IDS filter[7] preserves the actual intensity on both sides of the edge in addition to the edge location (the one crossing location). This filter also preserves the reflectance ratio (Weber fraction) at the edge location. Therefore, we can recover the intensity levels between the edge boundaries as well as the (relative) reflectance representation.

Our recovery method is local and uses the information contained in each edge element explicitly, recursively and independently. Therefore, this recovery process is quick and practical, with no need for extra memory, other than the storage for the recovered image itself, nor any extra calculations or processing.

2. PRIMITIVE EXTRACTION FROM THE LAPLACIAN OF GAUSSIAN FILTER

A. The $\nabla^2 G$ Filter

The model of lateral inhibition in early human vision processing and the assumption of white stationary Gaussian noise as a model for the natural noise source motivated Marr and Hildreth[6] to develop the spatially invariant $\nabla^2 G$ operator

$$\tau(x, y; \sigma) = \frac{1}{\pi\sigma^4}\left(1 - \frac{r^2}{2\sigma^2}\right)\exp\left(-\frac{r^2}{2\sigma^2}\right), \tag{1}$$

where $r^2 = x^2 + y^2$ and σ is the standard deviation of a normal distribution (Fig. 2). It is convenient to normalize the spatial variables relative to the sampling interval. Thus, for $\sigma = 1$, the standard deviation of the Gaussian is equal to the sampling interval.

The Gaussian is the only filter that guarantees a nice scaling behavior of the zero and level crossings of the linear differential operators.[4] It also is localized simultaneously and optimally in the spatial and spatial-frequency domains. The $\nabla^2 G$ operator is a linear isotropic bandpass filter that inherently satisfies the proper sequence of smoothing and differentiating for ill-posed differentiation problems (i.e., differentiating noisy data), and it assures smooth and stable zero-crossing curves.[8]

B. Step Edge Response

Isotropic filters allow a one-dimensional change of intensity from I to $I+\Delta I$ to simulate an ideal step edge. The response of this edge to the $\nabla^2 G$ filter, as given by

$$S_\sigma(x;\sigma,\Delta I) = \frac{\Delta I \cdot x}{\sqrt{2\pi}\sigma^3} \exp\left(-\frac{x^2}{2\sigma^2}\right), \tag{2}$$

is the familiar Mach-band pattern around the edge boundary that crosses zero exactly at the location of the change of the intensity. The corresponding peak and trough are symmetrically located at $x = \sigma$ and $x = -\sigma$ taking the values of

$$S_\sigma(\pm\sigma) = \pm\frac{\Delta I}{\sqrt{2\pi e}\sigma^2}. \tag{3}$$

The corresponding change of intensity becomes

$$\Delta I = \frac{\sqrt{2\pi e}\sigma^2[S_\sigma(\sigma) - S_\sigma(-\sigma)]}{2}. \tag{4}$$

Consequently, we have shown that the bandpassed data preserves the edge location and the change of intensity across it for spatial details that are at least 3σ wide (ideal case). Thus, when the bandpassed data $S_\sigma(x,y)$ is the only information available, the change of intensity associated with each edge element may become part of the image primitives in the low-level processing. The low-level processing consists of (1) detecting the zero-crossing location (x_o, y_o), (2) estimating the local edge direction θ, (3) measuring the values of $S_\sigma(x,y)$ at the points $(x_o \pm \sigma\sin\theta,\ y_o \pm \sigma\cos\theta)$, and (4) recovering ΔI using Eq. (4). The primitives (x_o, y_o), θ, and ΔI are used later to recover the (relative) intensity of the original image.

For the nonideal case, where a detail is insufficiently coarse relative to the spread of the filter, or where two edges cross each other or form a corner, it may often be possible to approximate ΔI. This approximation is achieved by measuring $S_\sigma(x,y)$ at the points $(x_o \pm r\sin\theta,\ y_o \pm r\cos\theta)$ where $r \leq \sigma$. Eq. (4) then takes on the form

$$\Delta I = \frac{\sqrt{2\pi}\sigma^3[S_\sigma(r) - S_\sigma(-r)]}{2r\exp\left(-\frac{r^2}{2\sigma^2}\right)} \tag{5a}$$

when $S(r)$ and $S(-r)$ are available and are approximately antisymmetrical and

$$\Delta I = \frac{\sqrt{2\pi}\sigma^3 S_\sigma(r)}{r\exp\left(-\frac{r^2}{2\sigma^2}\right)} \quad \text{or} \quad \Delta I = \frac{\sqrt{2\pi}\sigma^3 S_\sigma(-r)}{-r\exp\left(-\frac{r^2}{2\sigma^2}\right)} \tag{5b}$$

when only $S_\sigma(r)$ or $S_\sigma(-r)$ can be reliably measured.

C. Normalized Response

The Mach-band patterns at different scales (different σ) differ from each other not only by their spreads but by their amplitudes as well. The bandpass filter can be normalized in such a way that the response of an ideal step edge to the $\nabla^2 G$ filters at different scales will have the same amplitude and will differ only in their spreads. The scale S_σ for which the amplitude of the Mach-band pattern is exactly ΔI [i.e., $\Delta I = S(S_\sigma) - S(-S_\sigma)$] can be obtained from Eq. (4) as

$$S_\sigma = \left(\frac{2}{\pi e}\right)^{1/4} \cong 0.69. \tag{6}$$

To maintain constant amplitude ΔI , regardless of the operator size (i.e., the choice of S_σ), the bandpassed image should be multiplied by the normalization factor σ^2/σ_o^2. Figure 3 shows the response of the different operator sizes to an edge after normalization. The amplitude of the Mach-band pattern is exactly ΔI for all the responses. The only difference between them becomes the distance between the peak and trough and the zero crossings.

Consequently, for the ideal case, we can extract the change of intensity ΔI from the normalized bandpassed data, S, by the relationship

$$\Delta I = S(\sigma) - S(-\sigma). \tag{7}$$

Similarly, for the nonideal case, we can extract ΔI from the relationship

$$\Delta I = \frac{2}{b} S(r) \exp\left(\frac{1 - b^2}{2b^2}\right), \tag{8}$$

where $b = \sigma/r$, and $r = \sigma$ refers to the ideal case.

The recovery of edge primitives obtained for the continuous and normalized response of an ideal edge to the $\nabla^2 G$ filter is in practice constrained by the sampling interval. This constraint is part of the imaging system and the inevitable transformation from continuous targets to their corresponding digital representations. It is interesting to observe that the scale σ_o corresponds to the size of the smallest scale with which edges can be reliably detected relative to the sampling interval of the image-gathering system. Therefore, σ_o determines the resolution of the recovery process. According to Marr et al.,[9] the smallest operator has a standard deviation $\sigma = 0.69$ relative to a normalized sampling interval. Furthermore, Huck et al.[10–12] have demonstrated that the resultant trade-off between aliasing and blurring in the image gathering for this response maximizes the acquired information density for high signal-to-noise ratios. The resolution of the recovery is constrained mostly by the sampling interval and not by the Gaussian blur represented by σ_o. In practice, it is preferable to let σ be 0.75 instead of 0.69. This slight increase in size appreciably reduces aliasing degradations for some signals.

D. The Recovery Process

The edge primitives extracted by the low-level processing just described, associated each edge point (x_o, y_o) with its local edge direction θ and its local change of intensity $\triangle I$. In this section we present a method for recovering the (relative) intensity representation of the original image from these primitives. At first, we assign one of the regions of the image with an arbitrary initial intensity value I_o. From this region onward, we spread the values of $I + \triangle I$ and I toward the peak and trough of the Mach-band pattern, namely, in the $(x_o \pm r \sin\theta,\ y_o \pm r \cos\theta)$ directions. Spreads from different edge points toward the same region are averaged. Consequently, the image is recovered constructively, starting from one of the regions of the image. Each edge point joining the process provides a step towards the final representation of the recovered image. Theoretically, one estimate per region is sufficient to recover its (relative) intensity. However, we use estimates from all the ideal edge elements to attenuate the local error of each estimate. The recovery can be correct only up to a shift constant that is a function of the difference between the initial value I_o and the true intensity that corresponds to this starting region. The recovery process is quick and practical. It does not need high-order polynomial representations to describe the image,[3,4] nor does it need any extra calculations after the primitives (x_o, y_o), θ, and $\triangle I$ are obtained. The only memory needed for the recovery is that of the recovered image itself in which the edge elements are represented with their associate extra information θ and $\triangle I$.

Our methodology extends the conditions for detecting stable edge curves from $\nabla^2 G$-bandpassed data set by Torre and Poggio.[8] They added to the zero detection from $S(x, y)$ the requirement that $|S(x, y)| \neq 0$ for the detected zero elements. Thus, a detector designed to extract zero crossings as edge elements from bandpassed images should also include information about the gradient of the bandpassed data near the detected zero crossings (usually referred to as slope). This additional information enables the detection of smooth and connected edge curves, defines corners in the image, and thresholds the noisy and disconnected elements from the true edge elements. In our low-level processing we changed the slope evaluation of the Mach-band pattern to its amplitude measurement. This slight change made the difference between the recovery of only the primal sketch description to the recovery of the intensities between these boundaries as well.

E. Accuracy and Stability

Inaccuracies in extracting the edge primitives introduced into the recovery process, even for an ideal case, are caused by the digital implementation of the (mathematically) continuous process. Further errors are introduced, in practice, by the image-gathering degradations (aliasing, blurring, and noise). It is necessary to choose the interval of processing (discretization interval) to be sufficiently small relative to both the sampling interval and σ, in order to minimize the inaccuracies of measuring $S(x, y; \sigma)$ and to assure stable estimates.

A recovery process that is based on estimates obtained from Eq. (7) or from Eq. (8) seems, initially at least, to be the same. However, estimating $\triangle I$ from Eq. (8) is like estimating it from $S'(x, y)$ (the gradient of $S(x, y)$), as opposed to the amplitude of $S(x, y)$, as we do in Eq. (7). The former estimation tends to be unstable, as was also observed by Hummel,[5] especially when the estimate is made for $r \ll \sigma$. The instability occurs because $S'(x, y) = \triangle I \cdot \nabla^2 G$ reaches its maximum at the edge location (x_o, y_o) which is near to where we measure $S(x, y)$ to approximate $\triangle I$ from Eq. (8) [Fig. 4(a)]. By contrast, $S'(x, y)$ is zero at $(x_o \pm \sigma \sin\theta,\ y_o \pm \sigma \cos\theta)$, where we measure $S(x, y)$ for the approximation obtained from Eq. (7). Small inaccuracies in measuring S near the edge location, where the gradient is the steepest, are amplified as a function of $\triangle I$ and result in large local errors when estimating $\triangle I$ (unstable recovery). On the other hand, small and local inaccuracies in measuring S near $r = \sigma$ are insignificant in the overall recovery (stable recovery).

The relative error in estimating $\triangle I$ from the Mach-band pattern is

$$\frac{\epsilon_{\triangle I}}{\triangle I} = \left[\left(1 - \frac{1}{b^2}\right)^2 + \frac{1}{\sigma^2} + \left(b + \frac{1}{b}\right)^2\right]^{1/2} \left(1 - \frac{1}{b}\right) \tag{9}$$

where $b = \sigma/r$, and r denotes the distance from the edge location to the location where S was measured. Fig. 4(b) illustrates the relative error $\epsilon_{\triangle I}/\triangle I$ as a function of $1 - 1/b$ and σ. As expected, the relative error is zero for $1 - 1/b = 0$ (i.e., at $r = \sigma$). Stable estimates can be obtained if the peak and trough of the Mach-band pattern are at a distance of at least three intervals of processing from the edge location (i.e., $3\triangle x = \sigma$ and $\triangle x$ denotes the interval of processing, $\triangle x \leq 1$). Hence, the relative error is stable up to $1 - 1/b = \triangle x/2\sigma, \triangle x/2\sigma = 1/6$, (i.e., $\sigma - r \leq \triangle x/2$ and $3\triangle x = \sigma$), and diverges when $1 - 1/b > \triangle x/2\sigma$. A value of $\triangle x/2\sigma = 1/6$ results in an interval of processing that assures smooth discrete representation of the continuous $\nabla^2 G$. For such an interval of processing, the local relative error in estimating $\triangle I$ is smaller than 30% [see Figs. 4(c) and 4(d) for an actual σ], and can be controlled by averaging all the estimates for a given region.

Therefore, for a stable recovery, we recommend (1) implementation of filtering and processing with a discretization interval $\triangle x \leq 1$ that also obeys $\triangle x/2\sigma \leq 1/6$, $\sigma \geq \sigma_o$ and (2) the use of the estimates of $\triangle I$ obtained by Eq. (7). Eq. (8) may be used only when the actual peak or trough location falls between two discrete intervals of processing. After the entire image is recovered and a region remains with no estimate at all for its (relative) intensity, only then is it recommended to use the estimates of Eq. (8) to complete the recovery process (optional second stage of recovery). That way, the (relative) intensity of some small spatial details might be inaccurate, but the error will be local with no further propagation.

3. PRIMITIVE EXTRACTION FROM THE INTENSITY-DEPENDENT SPATIAL SUMMATION FILTER

A. The IDS Filter

Adaptive response to the intrinsic noisiness of light (photon noise) in early human vision processing motivated Cornsweet and Yellott[7] to develop the IDS filter. The IDS model consists of nonnegative, spatially homogeneous, circularly symmetric spread functions (SF) K, with unity volumes. The SF's differ from each other by their spreads, which are inversely dependent on the local intensity $I(x, y)$ as given by

$$\tau(x, y; I) = IK(Ir^2) \tag{10}$$

where $r^2 = x^2 + y^2$. Thus, the effect of the input intensity is to rescale the SF's, leaving their basic form unchanged [Fig. 5(a)]. The image response to the IDS model is the sum of the SF's [Fig. 5(b)]:

$$S(x, y; I) = \iint_{\infty}^{-\infty} \tau(x', y'; I) dx' dy'. \tag{11}$$

The IDS operator is an isotropic spatially variant bandpass filter that exhibits the following properties:

(1) Its response to a nonzero uniform scene is unity

(2) Its response is invariant under translation and rotation

(3) Its response to an input intensity $cI(x, y)c > 0$ is

$$S[x, y; cI(x, y)] = S\left[x\sqrt{c},\ y\sqrt{c}; I\left(x/\sqrt{c},\ y/\sqrt{c}\right)\right]$$

That is, the height of the SF is increased by the factor c while its width is decreased by the factor $1/\sqrt{c}$ (scaling property).

In the discrete digital implementation, c is chosen so that the diameter of the SF for the highest intensity of the image overlaps with at least seven discrete image data. The distance between these data is then assumed to be $1/\sqrt{c}$. It can be interpreted as the physical separation between the sampled data (i.e., the sampling interval), or as the discretization of the continuous IDS model given by Eq. (11) (i.e., the interval of processing).

B. Step Edge Response

For the recovery purpose, we restrict ourselves to the family of feasible SF's for the IDS filter that are also separable. Similar to the response of an ideal step edge to the $\nabla^2 G$filter, the edge response to the IDS filter, as given by

$$S(x;I,\triangle I) = 1 + \int_0^{\sqrt{I+\triangle I}x} K(z)dz - \int_0^{\sqrt{I}x} K(z)dz = S\left(\sqrt{I}x;1,W\right), \tag{12}$$

is a Mach-band pattern around the edge boundary. $W = \triangle I/I$ denotes the Weber fraction or the reflectance ratio. The Mach-band pattern crosses the value of one exactly at the edge location. The corresponding peak and trough are located symmetrically at a distance p that satisfies the equation

$$\sqrt{1+W}K\left(\sqrt{1+W}p'\right) = K(p') \tag{13}$$

where $p' = \sqrt{I}p$, and they take on the value $S(p';1,W)$. The range of the amplitude of the Mach-band pattern is dictated by the unity volume condition of the SF's and is given by $1 - 0.5 < S(\sqrt{I}p;1,W) < 1 + 0.5$. The amplitude reaches its limits $1 > 0.5$ when $I \to \infty$. The IDS response has a constant amplitude for a constant reflectance ratio W, while its spread is also a function of the original intensities I and $I + \triangle I$ (Fig. 6).

The IDS-bandpassed data $S(x,y;I,\triangle I)$ retains information about the original image. Thus, the original intensities on both sides of the edge and the reflectance ratio associated with each edge element may become a part of the image primitives in the low-level processing. The reflectance ratio is recovered by measuring the amplitude of the Mach-band pattern and deriving W from Eq. (12). The original intensities are recovered by measuring the distance from the peak and trough locations to the one-crossing location. Substituting these distances and the estimation of W in Eq. (13) and solving it, we extract the I and $I + \triangle I$ primitives needed for the recovery.

C. Recovery From the Cylindrical IDS Response

The cylindrical function is a feasible SF for the IDS-recovery process. Its definition is

$$K(x,y) = \begin{cases} 1 & 0 \le \sqrt{x^2+y^2} \le 1/\sqrt{\pi} \\ 0 & \text{elsewhere} \end{cases}$$

while its corresponding line spread function is

$$K(x) = \begin{cases} 2\left(\frac{1}{\pi} - x^2\right)^{1/2} & 0 \le x \le 1/\sqrt{\pi} \\ 0 & \text{elsewhere} \end{cases}$$

We have chosen to analyze the IDS recovery process with the cylindrical SF for the following reasons:

(1) The cylindrical SF has a finite support. Therefore, the spread of the corresponding IDS operator is finite with a radius of $(\pi I)^{-1/2}$. Finite support assures accurate integration in the

discrete implementation of Eq. (12). SF's with an infinite support, such as the Gaussian, typically would require more than twice the processing to approach the same numerical accuracy, due to the larger support necessary for the integration. Accurate integration is mandatory to a stable recovery process, as we will show in subsection E.

(2) The primitives can be extracted explicity from the cylindrical-IDS Mach-band pattern, i.e., through a direct relationship between the Mach-band amplitude and the primitives. Primitives can be extracted only implicity from the Gaussian-IDS Mach-band pattern, i.e., through look-up tables.[7]

Substituting the cylindrical SF in Eq. (13), and solving it for p, we have the distance from the one crossing (edge location) to the peak location in the Mach-band pattern as

$$p = [\pi I(2 + w)]^{-1/2}. \tag{14a}$$

The corresponding peak value derived from Eq. (12) takes on the value of

$$S(p) = 1 + \frac{1}{\pi}\sin^{-1}\left(\frac{W+1}{W+2}\right)^{1/2} - \frac{1}{\pi}\sin^{-1}\left(\frac{1}{W+2}\right)^{1/2} \tag{14b}$$

Consequently, the low-level processing consists of estimating the local edge direction θ at the one-crossing location (x_o, y_o), and measuring the peak and trough values $S(p)$ at their corresponding locations $(x_o \pm p\sin\theta, y_o \pm p\cos\theta)$. We can then recover the original ideal edge parameters (edge primitives) $W = \triangle I/I$, I, and $\triangle I$, using the bandpass signal information (i.e., p and $S(p)$) from the relationships

$$W = \frac{2\sin\phi}{1-\sin\phi}, \quad I = [2p^2(W+2)]^{-1}, \quad \triangle I = WI \tag{15}$$

where $\phi = \pi[S(p) - 1]$ for the peak measurements and $\phi = \pi[1 - S(p)]$ for the trough measurements. The primitives (x_o, y_o), θ, W, and I are used later to recover the (relative) reflectance and the intensity representations of the original image.

D. The Recovery Process

The recovery process from the IDS-bandpassed data is similar to the recovery process described for the $\nabla^2 G$-bandpassed data. The initial low-level processing associated each edge point (x_o, y_o) with its local edge direction θ, local reflectance ratio W, and local intensities I and $I + \triangle I$. Spreading these primitives onto their corresponding region in a similar process described in Section 2.D would result in the original intensity representation and the (relative) reflectance representation. The latter representation can be correct only up to a constant factor that relates to the initial reflectance that started the spread processing.

E. Resolution Accuracy and Stability

Resolution

The discrete display elements of the input data $I(x_i, y_i)$ determine the discretization intervals of the discrete IDS-bandpassed output image $S(x_i, y_i)$. The scaling property of the IDS helps us understand the transformation between the continuous representation of the IDS model and the discrete representation of the image data. We choose the scaling c so the diameter of the smallest spread of the IDS operator (e.g., at the highest intensity) will overlap at least seven discrete image elements. Thus, the distance between two discrete elements $\triangle x$ (smaller or equal to the sampling interval) has a physical distance of $\triangle x = 1/\sqrt{c}$. Therefore, when we measure the distance p in terms of intervals of processing, we should multiply it by $1/\sqrt{c}$ to be able to use Eq. (15) that was derived from the continuous representation of the IDS model. We do the same when we assess the resolution of the image recovery process.

The distance $p_{\triangle x}$ between the edge and peak locations in terms of intervals of processing is $[\pi \triangle x\ I(2+W)]^{-1/2}$. For images that are sufficiently sampled, features larger than $2p_{\triangle x}$ can be reliably recovered with the primal sketch description, along with the recovery of the (relative) reflectance or intensity representations. Spatial features smaller than $2p_{\triangle x}$ are blurred by the filter. Fig. 7 illustrates the resolution of the recovery for each intensity as a function of the scaling parameter c for a given reflectance ratio W.

Accuracy

The accuracy with which the reflectance ratio W can be recovered depends on the accuracy with which the peak and trough values of $S(x, y)$ are measured:

$$\epsilon_W = \frac{2\pi \cos\phi}{(1-\sin\phi)^2}\epsilon_s = \pi(W+2)\sqrt{W+1}\epsilon_s,$$

where $\phi = \pi[S(p) - 1]$. The peak and trough curves of the Mach-band pattern are parallel to the edge curve. Therefore, a small error in estimating the local edge direction θ, which determines the search direction for the peak and trough, does not affect the value $S(p)$. Moreover, if for an accurate θ, the actual peak or trough falls between two intervals of processing, then one of the neighboring elements is often a better measurement that can be obtained easily. Therefore, the error ϵ_s depends mostly on the quantization used in the digital implementation of the IDS (8 bits in our case) and is less than 30% for $0.2 < W < 128$ (on the [0,255] range), assuring a stable recovery [Fig. 8(a)].

The recovery of the original intensity, on the other hand, depends strongly on the accuracy with which the distance p is measured. The dual relationship between I and p as given by $\pi I p^2(2+W) = 1$, leads to the relative error ϵ_I/I in estimating I. For a measured distance p and an estimated W through a measurement of $S(p)$ the relative error is

$$\frac{\epsilon_I}{I} = \left[\pi^2(1+W)\epsilon_s^2 + 4\pi I(W+2)\epsilon_p^2\right]^{1/2},$$

where $\epsilon_p^2 \leq 1/4c$ [Figs. 8(b) to 8(d)]. The second term of ϵ_I/I is the dominant one. It can become high for orientations θ that do not agree with the rectangular lattice or parameters c that are not high enough. On the other hand, choosing a higher c would further blur the fine details so they would be unrecoverable. The scaling parameter c, which sets the limitation on the resolution of the recovery clearly demonstrates the usual trade-off between higher resolution (smaller c) and the accuracy of the recovery that can be obtained by increasing c [Figs. 7 and 8]. Accurate intensity recovery depends strongly on the type of the original scene and on the digital implementation of the IDS operator. Initial inaccuracy in the integration will further degrade the estimates of I due to errors in determining the one crossings and the distortion of the symmetry of the Mach-band pattern around it.

Stability

For each edge element that we recover from the IDS-bandpassed data we have two estimates for both the reflectance ratio W and the original intensity I [Eq. (15)]. One estimate is from measuring p and $S(p)$ at the peak of the Mach-band pattern, and the other one is from measuring p and $S(p)$ at the trough of the Mach-band pattern. We consider an estimate of W or I to be stable when the estimation through the peak and trough are about the same. The estimation that we use for the recovery process is the average of the two. Unstable estimates may occur when:

(1) The feature that we try to recover is smaller than $2p_{\triangle x}$

(2) Two Mach-band patterns interfere (corners, crossings, etc.)

(3) Edge orientation causes large inaccuracies in measuring p

(4) The reflectance ratio W is too high

For a stable recovery we go through a process that is similar to the $\nabla^2 G$recovery. We begin recovering the original image using only the stable estimates obtained from the IDS-bandpassed data. After the entire image is recovered and a region remains with no estimate at all for its reflectance or intensity (depends on which representation we wish to recover), only then do we use the unstable estimates to complete the recovery process. For images that are sufficiently sampled, regions with no stable estimate are minimal. While all we need is one stable estimate to recover a feature without using unstable estimates, we actually have stable estimates (that are averaged for smooth appearance) from most of the edge elements. The intensity recovery, although stable for images that are sufficiently sampled, tends to be less accurate than the (relative) reflectance recovery due to the inevitable discretization process.

4. RESULTS

In this section we characterize the images that are recovered from both the $\nabla^2 G$ and IDS-bandpassed signals without the use of any other data. The original image data are either computer-generated or obtained from a mock setup in space. Together these targets present a variety of different scene characteristics. These results combine the accuracy and stability assessments for a full recovery and the trade-offs for cases when only partial recovery can be obtained.

Figure 9 summarizes the recovery of image characteristics from the bandpassed data. The original targets are computer generated targets with features that are coarse enough relative to the sampling interval. The bull's-eye target that simulates staircase edges allows us to examine how constant change in the edge direction affects the quality of the recovery. The square target which is tilted 30 ° relative to the lattice allow us to examine how this tilt affects the recovery. The square and the random rectangles targets also allow us to examine how corners and crossings in a full range intensity image affect the recovery process. The spread of the $\nabla^2 G$ filter used herein was controlled by $\sigma = 1.0$ and the spread of the cylindrical IDS was controlled by $c = 6000$.

Using only the bandpassed data, the first stage in the recovery process is to extract the location of the intensity transitions (edges) through the zero crossing of the $\nabla^2 G$-bandpassed data or the one crossings of the IDS-bandpassed data. The resulting primal sketches are illustrated in Fig. 9(b). The recovery of the (relative) intensity representation from the $\nabla^2 G$-bandpassed data is illustrated in Fig. 9(c). The quality of the recovery is measured by the cross correlation ρ between the original target and the recovered one. The recovery of the intensities and the (relative) reflectance representations from the IDS-bandpassed data are illustrated in Figs. 9(d) and 9(e), respectively. As expected from the accuracy assessment, the quality of the (relative) reflectance recovery is better than the IDS intensity recovery. The high correlations between the original targets and the recovered ones suggest that the recovery process may be used as a decoder for a coding scheme in which only the edge primitives are transmitted.

Figure 10 illustrates a particularly important characteristic of the IDS filter, namely, the robustness of its reflectance representation to local variation in illumination (e.g., shadow). The recovered target [Fig. 10(d)] resembles the original [Fig. 10(a)], and not the shadowy [Fig. 10(b)], which is the one that was filtered. Traces of the shadow degradation can be seen in the modest loss of accuracy in the actual transition as the illumination decreases.

Figure 11 illustrates the capability of the recovery process with an experimental setup that simulated imaging conditions in space. The target examines the recoverability of targets with a wide dynamic range of intensities, in particular, the recoverability of spatial details under direct illumination or in deep shadow. As can be observed from the edge recovery representation [Fig. 11(b)], many important features of target, including features in deep shadow, could be recovered. The recoveries from the $\nabla^2 G$ (with $\sigma = 3.0$) are illustrated in Fig. 11(c), and those from the IDS (with $c = 6000$) are illustrated in Fig. 11(d) and Fig. 11(e). These recoveries resemble a slightly blurred version of the original target [Fig. 11(a)]. As could be expected from the accuracy and stability analysis, features that were relatively small produced inaccuracies as well as features with abrupt and steep changes in the intensities. Nevertheless, in most of the cases, these inaccuracies were contained within their regions with no further propagation.

5. CONCLUDING REMARKS

Assessment of the response of an ideal edge to a bandpass filter reveals that most of the target's characteristics are preserved. For applications that use bandpass signals, the recovery of those characteristics exhibits new dimensions to image understanding. Minimal extra processing is required, beyond that is needed for the primal sketch extraction process. The processing is based on the existing bandpassed data information and on the same storage needed for the recovered image itself. The potential for high data compression applications, transmitting only the information associated with detectable edge boundaries

(edge primitives), might be helpful when high data rate transmission is required. In light of our results and the stability assessment, we feel that the edge primitives information extracted from the bandpassed image is a good form of representation for images that are sufficiently sampled and properly processed.

REFERENCES

1. T. N. Cornsweet, *Visual Perception*, Academic Press, New York, 1970, pp. 277 and 304.

2. B. F. Logan, "Information in the zero crossing of bandpass signals", The Bell System Technical Journal, Vol. 56, No. 11, pp. 487-510, 1977.

3. S. R. Curtis, A. V. Oppenheim, and J. S. Lim, "Signal reconstruction from Fourier transform sign information", IEEE Trans. on Acoustics, Speech and Signal Processing, Vol. ASSP-33, No. 3, pp. 643-657, June 1985.

4. A. L. Yuille and T. Poggio, "Fingerprints theorems for zero crossings", J. Opt. Soc. Am., Vol. 2, No. 5, pp. 683-692, 1985.

5. R. A. Hummel, "Representations based on zero crossings in scale-space", IEEE Proc. of the Computer Vision and Pattern Recognition Conference, pp. 204-209, June 1986.

6. D. Marr and E. Hildreth, "Theory of edge detection", Proc. R. Soc., London B 207, pp. 187-217, 1980.

7. T. N. Cornsweet and J. I. Yellott, Jr., "Intensity-dependent spatial summation", J. Opt. Soc. Am., 2, pp. 1769-1786, 1985.

8. V. Torre and T. A. Poggio, "On edge detection", IEEE Trans. Pattern Anal. Machine Intell., PAMI-8, pp. 147-163, 1986.

9. D. Marr, T. A. Poggio, and E. Hildreth, "Smallest channel in early human vision", J. Opt. Soc. Am., Vol. 70, No. 7, pp. 868-870, July 1980.

10. F. O. Huck, C. L. Fales, D. J. Jobson, S. K. Park, and R. W. Samms, "Image-plane processing of visual information", Applied Optics, Vol. 23, No. 18, pp. 3160-3167, 1984.

11. F. O. Huck, C. L. Fales, N. Halyo, R. W. Samms, and K. Stacey, "Image gathering and processing: Information and fidelity", J. Opt. Am. A2, pp. 1644-1666, 1985.

12. F. O. Huck, C. L. Fales, J. A. McCormick, and S. K. Park, "Image-gathering system design for information and fidelity", J. Opt. Soc. Am. A5, pp. 285-299, 1988.

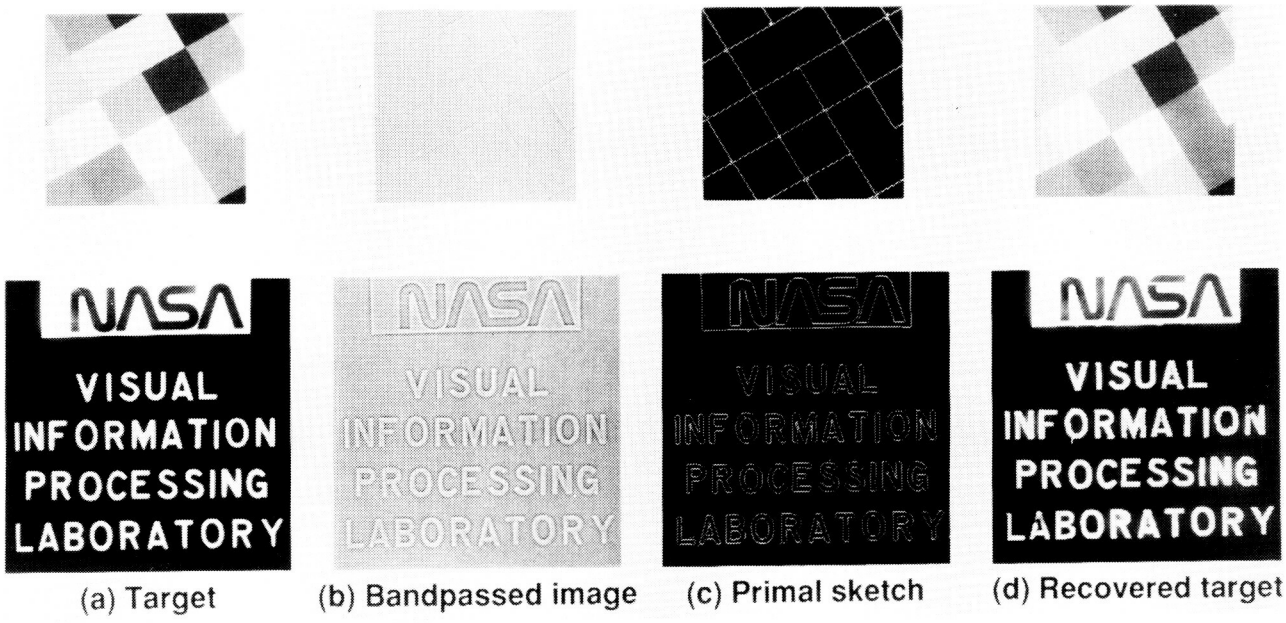

Figure 1: The recovery process from the bandpassed representation to the original image representation.

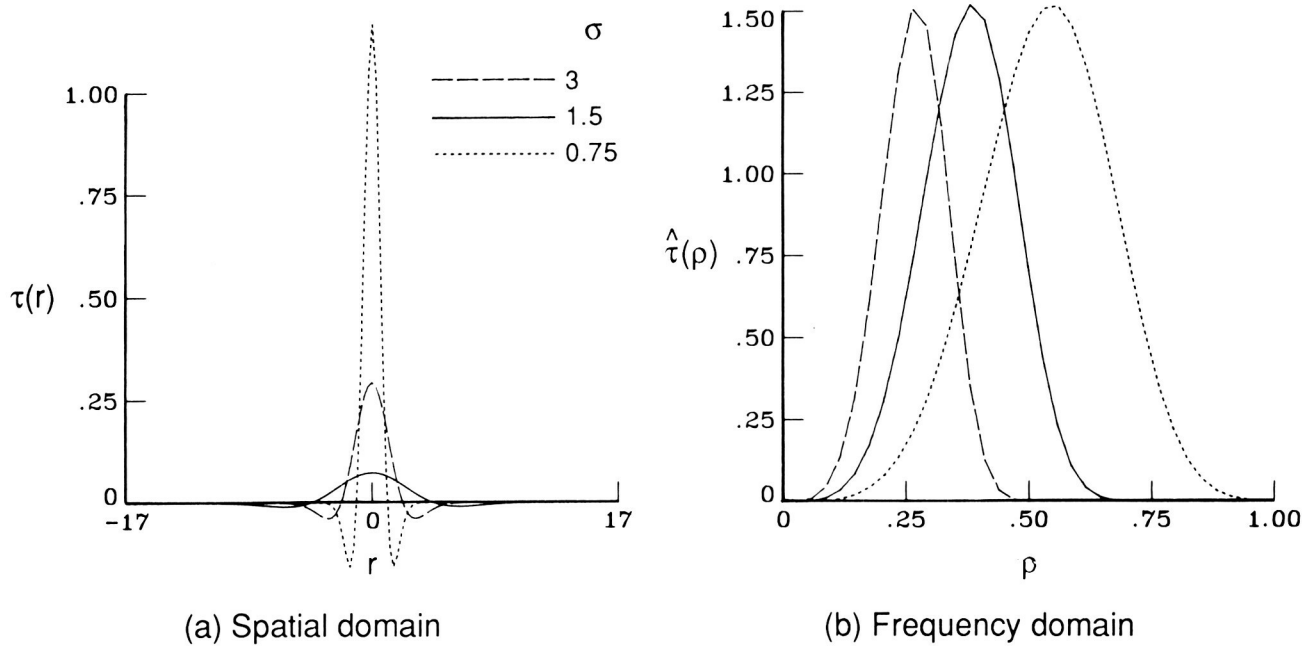

Figure 2: Normalized $\nabla^2 G$ response for three standard deviations σ.

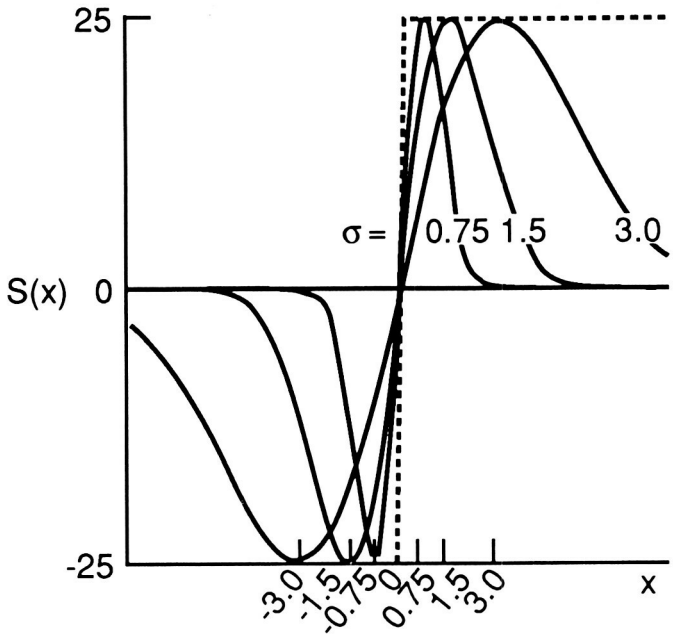

Figure 3: Normalized response to an ideal step edge for $\nabla^2 G$ operators with different σ.

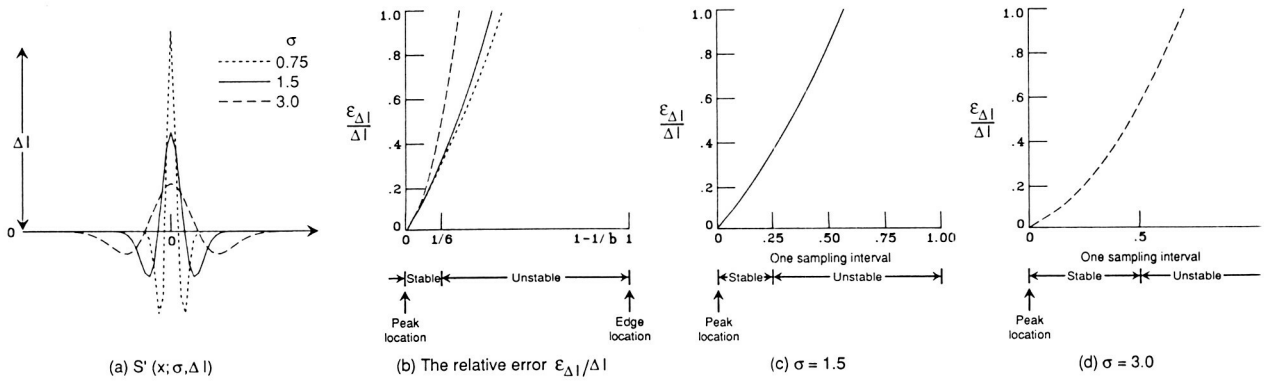

Figure 4: Accuracy of the $\nabla^2 G$ recovery process.

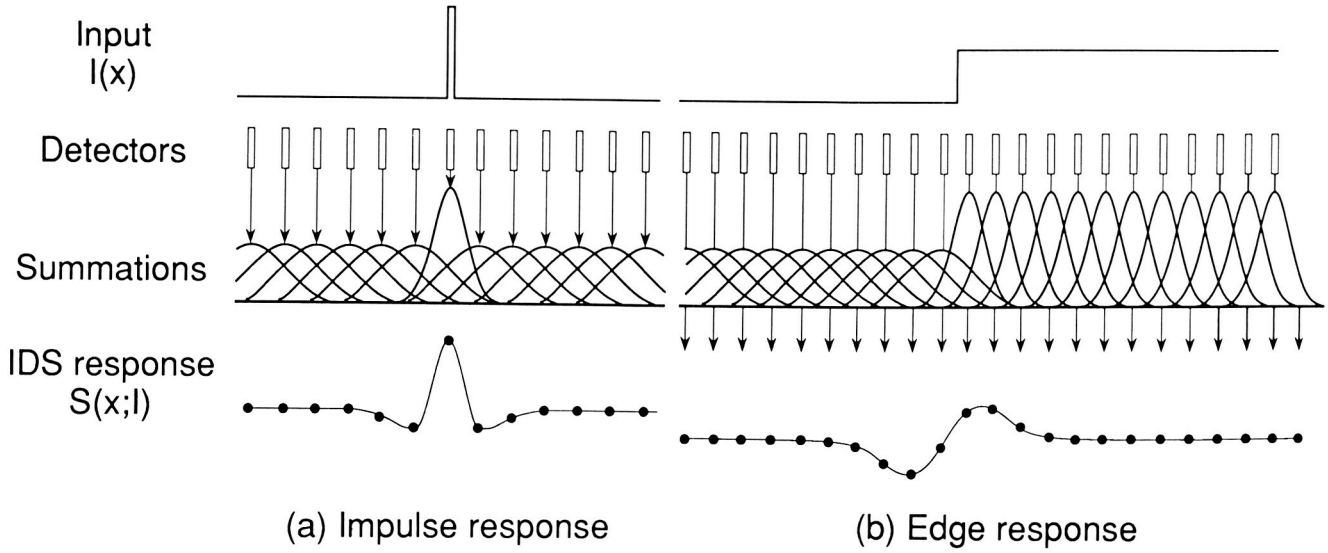

Figure 5: The IDS response.

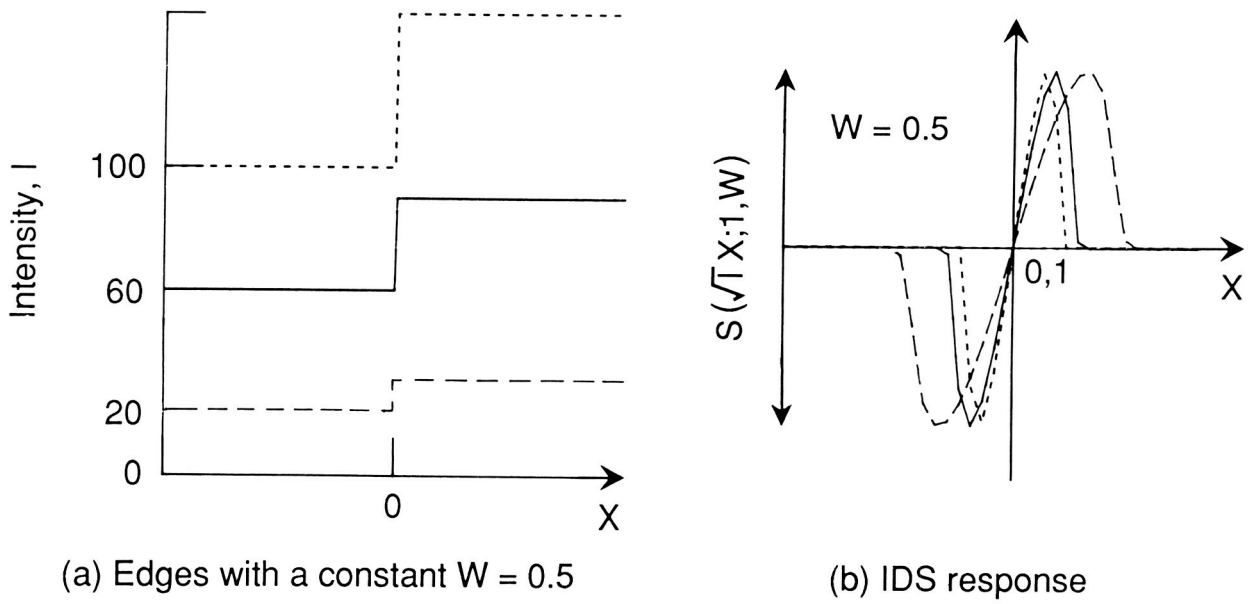

Figure 6: Response of ideal step edges to the IDS operator.

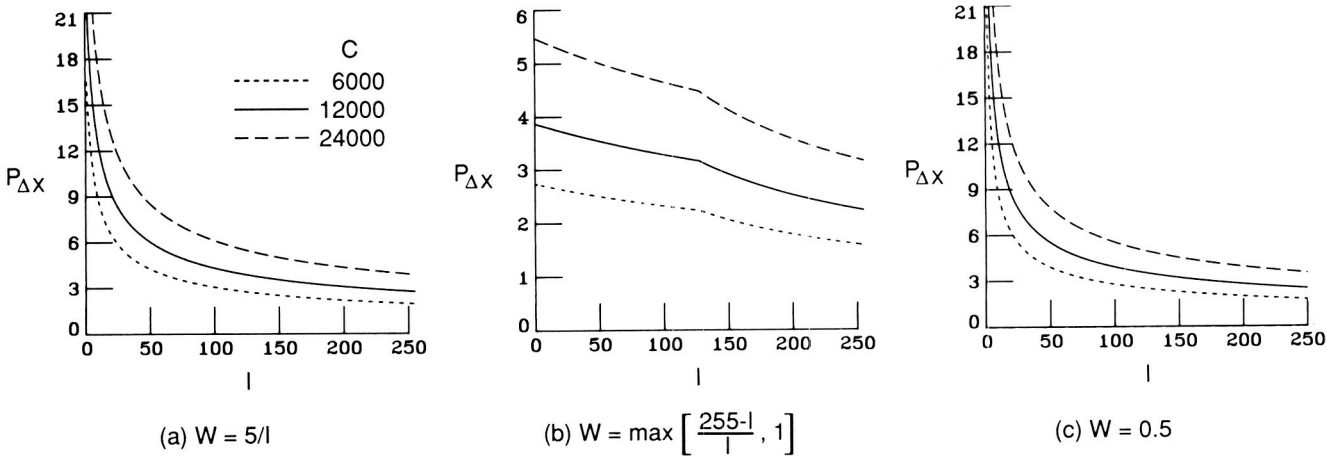

Figure 7: Resolution of the IDS recovery process.

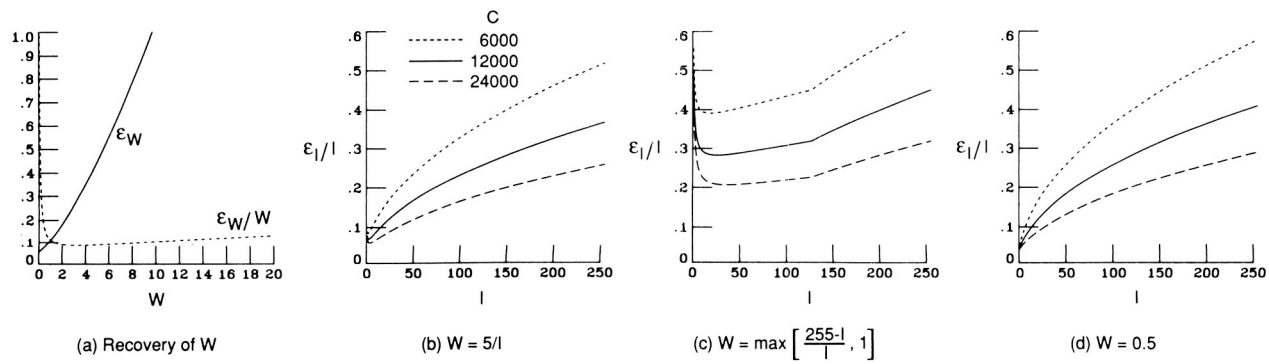

Figure 8: Accuracy of the IDS recovery process.

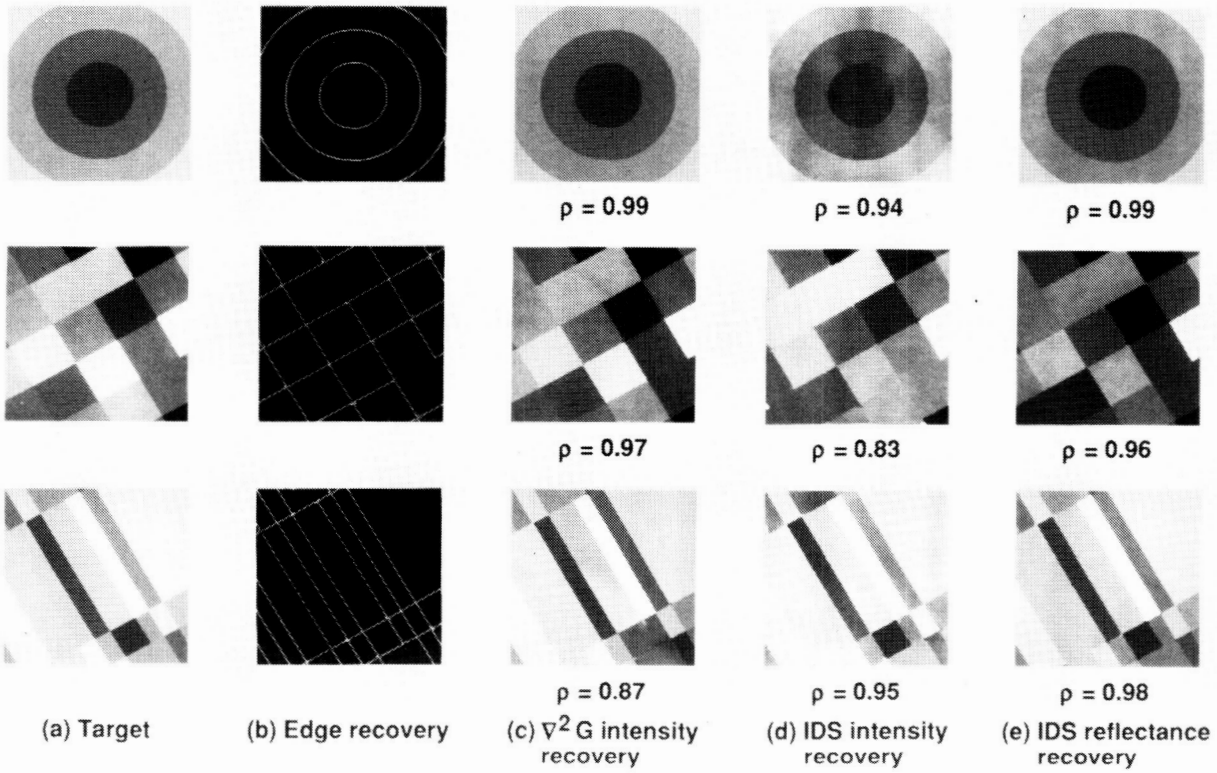

Figure 9: The recovery process for computer-generated targets.

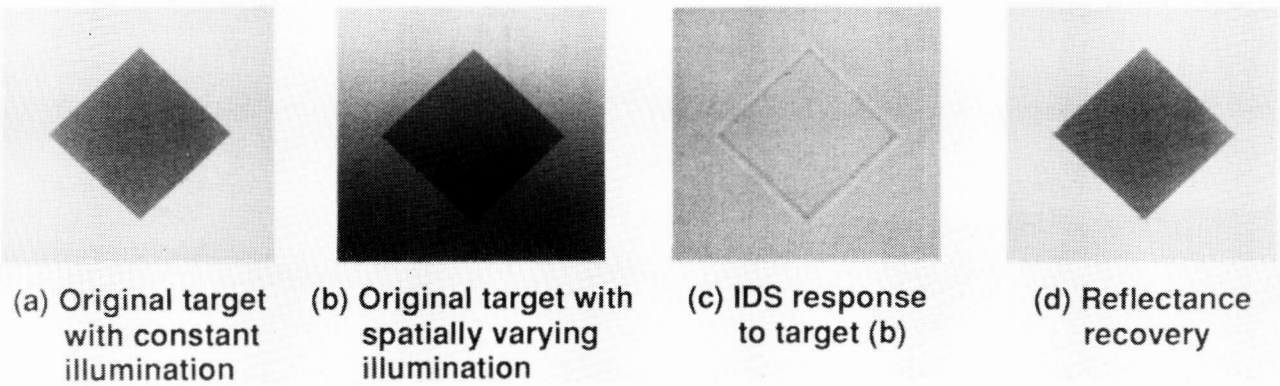

Figure 10: Recovery from spatially varying illumination.

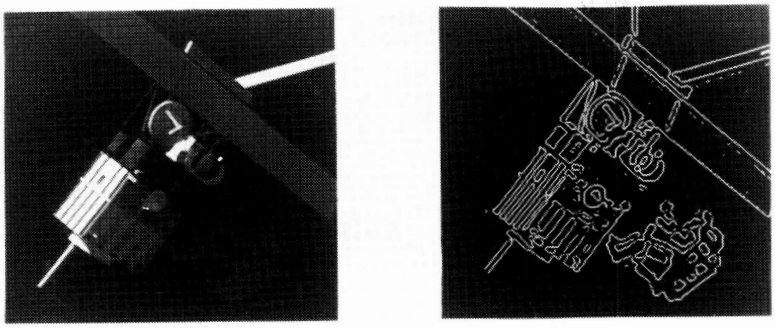

(a) Target (b) Edge recovery

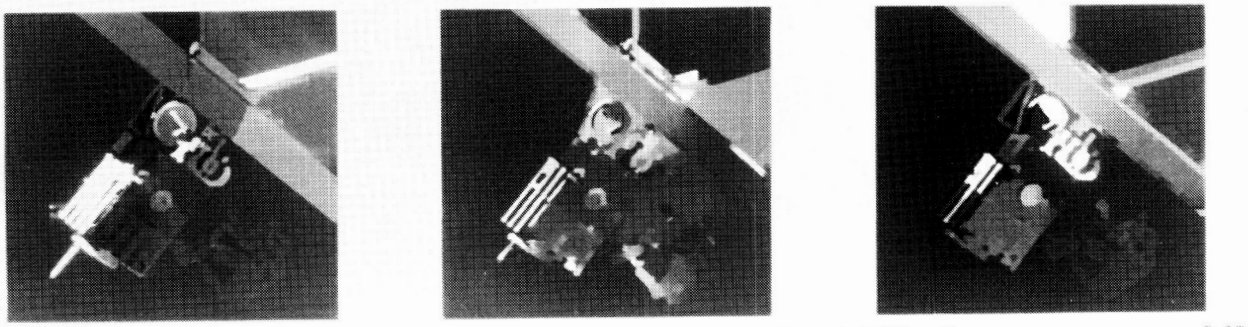

(c) $\nabla^2 G$ intensity recovery. $\rho = 0.84$ (d) IDS intensity recovery. $\rho = 0.45$ (e) IDS reflectance recovery. $\rho = 0.42$

Figure 11: Feature extraction for an experimental image that simulates imaging conditions in space.